ELSEVIER

PII: S0266-3538(97)00078-X

*Composites Science and Technology* **58** (1998) 19–29

Printed in Northern Ireland
0266-3538/98 $19.00

# MECHANICAL BEHAVIOUR OF ±55° FILAMENT-WOUND GLASS-FIBRE/EPOXY-RESIN TUBES—III. MACROMECHANICAL MODEL OF THE MACROSCOPIC BEHAVIOUR OF TUBULAR STRUCTURES WITH DAMAGE AND FAILURE ENVELOPE PREDICTION

Gengkai Hu,† JinBo Bai,* Ekaterina Demianouchko & Philippe Bompard

*Laboratory MSS/MAT, CNRS URA 850, Ecole Centrale de Paris, 92295 Châtenay Malabry Cedex, France*

(Received 15 April 1996; revised 21 March 1997; accepted 28 April 1997)

**Abstract**

*This series of papers on ±55° filament-wound glass-fibre/epoxy-resin tubes consists of three parts. In the present paper (Part III), the macroscopic mechanical behaviour of the tubular structure is presented. A method for predicting composite tube macroscopic properties from the ply constants is given. A more general analytical method is used for determining ply stresses of a composite tube under a combined load, which will then be compared with 3D finite-element analysis, classical and adjusted laminate theory. Failure envelope prediction is then made according to the micro- and meso-scale model results. The stresses distribution in the tube thickness direction predicted by the present method agrees well with 3D finite-element analyses. Four methods give similar stress distribution results under tensile loading, but different ones under internal pressure loading. For failure envelope prediction, the first-ply-failure theory underestimates the failure load for pressure dominated loading. The effect of possible micro structural damage on the failure load prediction is also discussed and compared with experimental results. In Part I (Bai* et al. Compos. Sci. Technol., *1997, **57**, 141–153), the microstructure, mechanical behaviour and damage initiation mechanisms were presented. In Part II (Bai* et al. Compos. Sci. Technol., *1997, **57**, 155–164), micromechanical modelling of the damage initiation was conducted in order to determine the mechanical conditions under which different microcracking mechanisms occur.* © *1998 Elsevier Science Ltd. All rights reserved*

*Keywords:* meso and macromechanical modelling, transverse cracking, delamination, stress analysis, failure criterion

*To whom correspondence should be addressed.
†On leave from Department of Applied Mechanics, Beijing Institute of Technology, People's Republic of China

## 1 INTRODUCTION

Extensive experimental investigations have been undertaken on ±55° filament-wound glass-fibre/epoxy-resin tubes.[1,3–14] Most studies were directed towards the prediction of failure envelopes for thin-walled cylinders with only a few wound layers. It was observed that tubes tested under biaxial loading conditions failed with greatly varying strengths, subsequently producing asymmetric biaxial failure envelopes (axial failure strength vs circumferential failure strength). The failure envelopes depend strongly on the winding angles. Filament-wound tubes with a winding angle of ±55° exhibit higher strength under combined loading.[5–7,9] Microscopic observations for failure mechanisms of filament-wound composite tubes under combined load were conducted by Jones *et al.*,[15] Carroll *et al.*[4] and Bai *et al.*,[1] and revealed them to be dependent on the applied stress ratio. In general, microcracking and delamination were the most readily observed damage mechanisms and any combination of the two constituted most failures. Two types of microcracking were established, notably cracking transverse to the fibre direction (transverse cracking) and cracking perpendicular to the loading direction in the resin-rich zones (matrix cracking). Transverse cracking is initiated at or near the fibre/matrix interface or at existing porosity and it propagates through the ply thickness. This damage mode is more frequently observed in the axial-loading-dominated region. In the internal-pressure dominated region, delamination is the main damage mode. It occurs more often between two adjacent layers. Prior to delamination, whitening of the tube is commonly observed.

The functional failure of a pressurised composite vessel or composite pipe in the form of leakage or weeping of the contained gas or fluid is critical as far as design and performance of the composite is concerned. The leakage failure of a filament-wound fibre-composite

vessel, subjected to a combined internal pressure and axial loading, is commonly viewed as a result of progressive damage produced by the coalescence of forming micro-cracks, creating a 'through-thickness' crack path prior to the complete loss of structural load bearing capability.[1,3] Furthermore, the weepage in a piping system, i.e. fluid penetration in the tube wall, can also alter the long-term behaviour of the composite (ageing effects, etc.).[10]

Theoretical predictions of failure envelopes for composite tubes under combined loading conditions have been proved unsuccessful. Hinton *et al.*,[5] basing their work on classical laminate theory and mesoscale criteria (Hill, maximum stress, Tsai-Wu), constructed failure envelopes for composite tubes with different winding angles. They found that all classical mesoscale criteria yielded predictions that were much too conservative, although prediction for axial loading conditions seemed acceptable.[5,13,14]

In our study, we shall consider a composite tube designed to transfer fluid for the cooling water, monitoring and fire system in nuclear power stations. It is made of six plies according to the lay-up sequence $(55°/-55°)_3$. Each laminate contains 56 vol% glass fibre (fibre: Young's Modulus $E = 73{\cdot}8$ GPa, Poisson ratio $\nu = 0{\cdot}23$) and epoxy resin (resin: $E = 3{\cdot}4$ GPa, $\nu = 0{\cdot}35$). The work is presented in three parts. In the current paper (Part III), macroscopic behaviour of the tubular structure with and without damage is presented. A method for predicting composite tube macroscopic properties (elastic constants for example) from its ply constants is given. A more precise analytical method is presented for determining ply stresses of a composite tube which is then compared with 3D finite-element analysis. With the determined stresses and a maximum stress criterion, the failure envelope of the composite tube will be evaluated and compared with the experimental values. The effect of damage on these predictions will also be discussed.

## 2 DETERMINATION OF STRESS FIELDS AT TUBE AND PLY SCALE

### 2.1 Analytical method

One of the concerns in structural design is the development of analytical or numerical methods for determining the responses under various loading conditions. The stress field of a single anisotropic cylinder layer due to mechanical loading was considered by Pagano.[16] For symmetric angle-ply composite tubes, Roy and Tsai[17] considered two symmetric plies as an orthotropic unit and evaluated the stress field of a composite tube under combined internal pressure and tension loading. With the help of Lekhnitskii's stress functions, Yuan[18] proposed a more precise analysis for a composite tube loaded by internal pressure. Recently Sayir and Motavalli[19] proposed an adjusted version of the laminate theory for stress analysis of composite tubes under uniform internal pressure. In our analysis, this method will be followed and modified in order to take into account axial loading. The results will be compared with those obtained by the classical laminate theory, the adjusted version of the laminate theory recently proposed by Sayir and Motavalli[19] and 3D finite-element method.

Consider a laminated cylindrical shell made of fibre-reinforced laminae and subjected to internal pressure and axial loading, where the free-end effect is neglected. It is assumed that the axis of anisotropy coincides with the longitudinal $x_3$ axis (as shown in Fig. 1).

The stress and engineering strain relationships in the tube reference (off-axis) for each ply can be expressed as

$$\begin{bmatrix} \varepsilon_{11} \\ \varepsilon_{22} \\ \varepsilon_{33} \\ \varepsilon_{23} \\ \varepsilon_{13} \\ \varepsilon_{12} \end{bmatrix} = \begin{bmatrix} S_{11} & S_{12} & S_{13} & S_{14} & & \\ S_{12} & S_{22} & S_{23} & S_{24} & & \\ S_{13} & S_{23} & S_{33} & S_{34} & & \\ S_{14} & S_{24} & S_{34} & S_{44} & & \\ & & & & S_{55} & S_{56} \\ & & & & S_{56} & S_{66} \end{bmatrix} \begin{bmatrix} \sigma_{11} \\ \sigma_{22} \\ \sigma_{33} \\ \sigma_{23} \\ \sigma_{13} \\ \sigma_{12} \end{bmatrix} \tag{1}$$

Connection between this off-axis ply compliance tensor and the compliance tensor $S_{ij}$ in the material reference ($x_1' x_2' x_3'$ as shown in Fig. 1) is given in Appendix 1. As a result of axisymmetric deformation, one can establish a system of coupled governing differential equations in terms of Lekhnitskii's stress functions for an individual lamina:[18]

$$L_4' F + L_3' \Psi = 0, \quad L_3'' F + L_2' \Psi = \frac{S_{34} A_3}{S_{33} r} - 2A_4 \tag{2}$$

where $A_3$ and $A_4$ are constants and the differential operators are defined as

$$L_4' = \tilde{S}_{22} \frac{\mathrm{d}^4}{\mathrm{d}r^4} + 2\tilde{S}_{22} \frac{1}{r} \frac{\mathrm{d}}{\mathrm{d}r^3} - \tilde{S}_{11} \frac{1}{r^2} \frac{\mathrm{d}^2}{\mathrm{d}r^2} + \tilde{S}_{11} \frac{1}{r^3} \frac{\mathrm{d}}{\mathrm{d}r}$$

$$L_3' = -\tilde{S}_{24} \frac{\mathrm{d}}{\mathrm{d}r^3} + (\tilde{S}_{14} - 2\tilde{S}_{24}) \frac{1}{r} \frac{\mathrm{d}^2}{\mathrm{d}r^2}$$

$$L_3'' = -\tilde{S}_{24} \frac{\mathrm{d}}{\mathrm{d}r^3} + (\tilde{S}_{14} + \tilde{S}_{24}) \frac{1}{r} \frac{\mathrm{d}^2}{\mathrm{d}r^2}$$

$$L_2' = \tilde{S}_{44} \frac{\mathrm{d}^2}{\mathrm{d}r^2} + \tilde{S}_{44} \frac{1}{r} \frac{\mathrm{d}}{\mathrm{d}r}$$

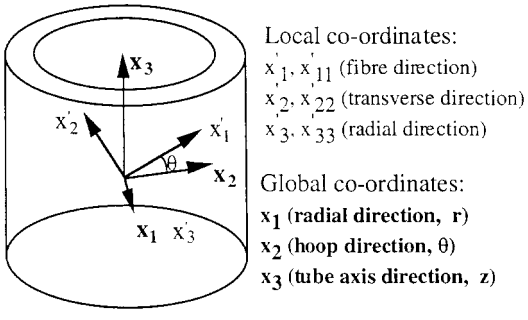


**Fig. 1.** Local and global reference systems.

and $\tilde{S}_{ij}$ the reduced compliance constants defined by $\tilde{S}_{ij} = S_{ij} - S_{i3}S_{j3}/S_{33}$ for $i, j = 1,2,4,5,6$. The stress components can be expressed as

$$\sigma_r = \kappa_1 A_3 + \kappa_2 A_4 r + (1+\mu_1) r^{\mu_1 - 1} C_1 + (1+\mu_2) r^{\mu_2 - 1} C_2 \tag{3}$$

$$\sigma_\theta = \kappa_1 A_3 + 2\kappa_2 A_4 r + \mu_1(1+\mu_1) r^{\mu_1 - 1} C_1 + \mu_2(1+\mu_2) r^{\mu_2 - 1} C_2 \tag{4}$$

$$\tau_{\theta z} = -\kappa_3 A_3 - \kappa_4 A_4 r - \mu_1 \eta_1 r^{\mu_1 - 1} C_1 - \mu_2 \eta_2 r^{\mu_2 - 1} C_2 \tag{5}$$

$$\sigma_z = l_1 A_3 + l_2 A_4 r - m_1 r^{\mu_1 - 1} C_1 - m_2 r^{\mu_2 - 1} C_2 \tag{6}$$

The displacement components are

$$u_r = d_1 A_3 r + d_2 A_4 r^2 + q_1 r^{\mu_1} C_1 + q_2 r^{\mu_2} C_2, \quad u_\theta = A_4 r z, \quad u_z = A_3 z \tag{7}$$

where

$$\eta_k = \frac{\tilde{S}_{14} + \tilde{S}_{24}\mu_k}{\tilde{S}_{44}} \frac{1+\mu_k}{\mu_k}, \qquad \mu_{1,2} = \pm \left( \frac{\tilde{S}_{11}\tilde{S}_{44} - \tilde{S}_{14}^2}{\tilde{S}_{22}\tilde{S}_{44} - \tilde{S}_{24}^2} \right)^{1/2} \tag{8}$$

and

$$\begin{aligned}
\kappa_1 &= [S_{34}(\tilde{S}_{24} - \tilde{S}_{14}) - \tilde{S}_{44}(S_{23} - S_{13})]/[\tilde{S}_{14}^2 - \tilde{S}_{24}^2) \\
&\quad - (\tilde{S}_{11} - \tilde{S}_{22})\tilde{S}_{44}]S_{33} \\
\kappa_2 &= (2\tilde{S}_{24} - \tilde{S}_{14})/[(\tilde{S}_{11} - 4\tilde{S}_{22})\tilde{S}_{44} - (\tilde{S}_{14}^2 - 4\tilde{S}_{24}^2)] \\
\kappa_3 &= [S_{34}(\tilde{S}_{22} - \tilde{S}_{11}) + (\tilde{S}_{24} + \tilde{S}_{14})(S_{13} - S_{23})] \\
&\quad /[(\tilde{S}_{14}^2 - \tilde{S}_{24}^2) - (\tilde{S}_{11} - \tilde{S}_{22})\tilde{S}_{44}]S_{33} \\
\kappa_4 &= (4\tilde{S}_{22} - \tilde{S}_{11})/[(\tilde{S}_{11} - 4\tilde{S}_{22})\tilde{S}_{44} - (\tilde{S}_{14}^2 - 4\tilde{S}_{24}^2)] \\
l_1 &= [1 - (S_{13} + S_{23})\kappa_1 + S_{34}\kappa_3]/S_{33} \\
l_2 &= -[(S_{13} + 2S_{23})\kappa_2 - S_{34}\kappa_4]/S_{33} \\
m_1 &= [S_{13}(1+\mu_1) + S_{23}(1+\mu_1)\mu_1 - S_{34}\eta_1\mu_1]/S_{33} \\
m_2 &= [S_{13}(1+\mu_2) + S_{23}(1+\mu_2)\mu_2 - S_{34}\eta_2\mu_2]/S_{33} \\
q_1 &= [\tilde{S}_{11}(1+\mu_1)/\mu_1 + \tilde{S}_{12}(1+\mu_1) - \tilde{S}_{14}\eta_1] \\
q_2 &= [\tilde{S}_{11}(1+\mu_2)/\mu_2 + \tilde{S}_{12}(1+\mu_2) - \tilde{S}_{14}\eta_2] \\
d_1 &= (\tilde{S}_{11} + \tilde{S}_{12})\kappa_1 - \tilde{S}_{14}\kappa_3 + S_{13}/S_{33} \\
d_2 &= [(\tilde{S}_{11} + 2\tilde{S}_{12})\kappa_2 - \tilde{S}_{14}\kappa_4]/2
\end{aligned} \tag{9}$$

The above solution applies to each individual ply. For a composite tube of $N$ layers, the unknown constants $A_3$, $A_4$, $C_1$, $C_2$ for the $k^{\text{th}}$ ply are determined by the following equations:

$$\sigma_r^k = \sigma_r^{k+1}, \quad u_r^k = u_r^{k+1}, \quad A_3^k = A_3^{k+1}, \quad A_4^k = A_4^{k+1} \quad \text{for} \quad k = 1, N-1 \tag{10}$$

and $\sigma_r^O = -p, \sigma_r^N = 0$ for internal pressure condition. For an axial load, they are replaced by the following equivalent resultant forces and moments

$$\int_A 2\pi\sigma_z r \, \mathrm{d}r \, \mathrm{d}\theta = F, \quad \int_A 2\pi\sigma_{z\theta} r^2 \, \mathrm{d}r \, \mathrm{d}\theta = 0 \tag{11}$$

where $F$ is the applied axial load and $A$ the area of tube cross section. $F = 0$ for pure internal pressure loading. The stress field in each ply can be obtained by solving the above equations.

### 2.2 Applications

An application of the method described above serves to determine the stress distribution for an angle ply composite tube. For the composite tube considered, the fibre volume fraction of unidirectional lamina is 0·56. The material constants of each ply are determined by a micromechanical model.[2] The internal radius of the composite tube is 30 mm, the thickness of each layer being 0·417 mm. The lay-up sequence of the composite is $(55°/-55°)_3$. The stress distribution in each ply in the case of pure internal pressure ($p = 10$ MPa, i.e. $\sigma_{\theta\theta} = 120$ MPa) is shown in Fig. 2(a). By transforming the stresses expressed in the tube reference into local ply co-ordinates, we obtain the results depicted in Fig. 2(b). In the case of axial loading ($F = 10$ kN, i.e. $\sigma_{zz} = 20{\cdot}37$ MPa), the stress distributions in different co-ordinates are illustrated in Fig. 3(a) and (b).

### 2.3 Comparison with other methods

*2.3.1 Comparison with the Adjusted Laminate Theory*

Recently Sayir and Motavalli[19] proposed a modified laminate method to evaluate stress distribution far from the free edges of a composite tube subjected to a pure internal pressure. The idea of this method is to use average ply stresses and strains. It is assumed that the longitudinal strain and the in-plane shear strains are constant throughout the tube thickness and length. Using average stress and strain in each layer, the $i^{\text{th}}$ ply's constitutive equation can be written as follows

$$\frac{u_1^i - u_1^{i-1}}{h_i} = S_{11}^i \frac{p_i + p_{i-1}}{2} + S_{12}^i \sigma_{22}^i + S_{13}^i \sigma_{33}^i + S_{14}^i \sigma_{23}^i \tag{12}$$

$$\frac{u_1^i + u_1^{i-1}}{2R_i} = S_{22}^i \frac{p_i + p_{i-1}}{2} + S_{22}^i \sigma_{22}^i + S_{23}^i \sigma_{33}^i + S_{24}^i \sigma_{23}^i \tag{13}$$

$$\varepsilon_{33} = S_{13}^i \frac{p_i + p_{i-1}}{2} + S_{23}^i \sigma_{22}^i + S_{33}^i \sigma_{33}^i + S_{34}^i \sigma_{23}^i \tag{14}$$

$$\varepsilon_{23} = S_{14}^i \frac{p_i + p_{i-1}}{2} + S_{24}^i \sigma_{22}^i + S_{34}^i \sigma_{33}^i + S_{44}^i \sigma_{23}^i \tag{15}$$

where $u_1^i$ is the radial displacement of the $i^{\text{th}}$ ply, $S_{ij}^k$ the $k^{\text{th}}$ ply's compliance tensor in the tube reference; $h_i$ the thickness of the $i^{\text{th}}$ layer; $R_i$ the radius from the middle of the $i^{\text{th}}$ ply to the tube centre; and $p_i$ the pressure applied on the $i^{\text{th}}$ layer, its value is known on the internal and external plies. The previous eqns together with the following global equilibrium relationships enable the determination of the unknown quantities:

$$\sum_{i=1}^{N} A^i \sigma_{33}^i = P_z + F \tag{16}$$

$$h_i \sigma_{22}^i = \left(R_i - \frac{h_i}{2}\right) p_{i-1} - \left(R_i + \frac{h_i}{2}\right) p_i \quad \text{for} \quad i = 1, N \tag{17}$$

$$\sum_{i=1}^{N} A^i \sigma_{23}^i = 0 \tag{18}$$

For comparison purpose, a tube of laminate sequence $(55°/-55°/55°/-55°)_s$ is considered. The material constants of each ply in the principle axis are

$$E_1 = 43{\cdot}8\,\text{GPa}, \quad E_t = 12{\cdot}5\,\text{GPa}, \quad G_1 = 4{\cdot}55\,\text{GPa},$$
$$G_t = 4{\cdot}55\,\text{GPa}, \quad v_t = 0{\cdot}31, \quad v_t = 0{\cdot}38$$

The inner radius of this tube is $R_0 = 33\,\text{mm}$ and the ply thickness is 0·53 mm. The stress distributions calculated by the two methods for both composite tubes are shown in Fig. 4.

The results in Fig. 4 exhibit some discrepancy. Adjusted laminated theory gives lower values than by our approach. The biggest difference is for the in-plane shear stress $\sigma_{zth}$. This is due to the global equilibrium conditions given in eqns (11) and (18). They will be further compared with 3D finite-element analysis which could be considered as reference case.

*2.3.2 Comparison with the Classical Laminate Theory*

The proposed theory is also compared with the classical laminate theory. The results for the studied composite

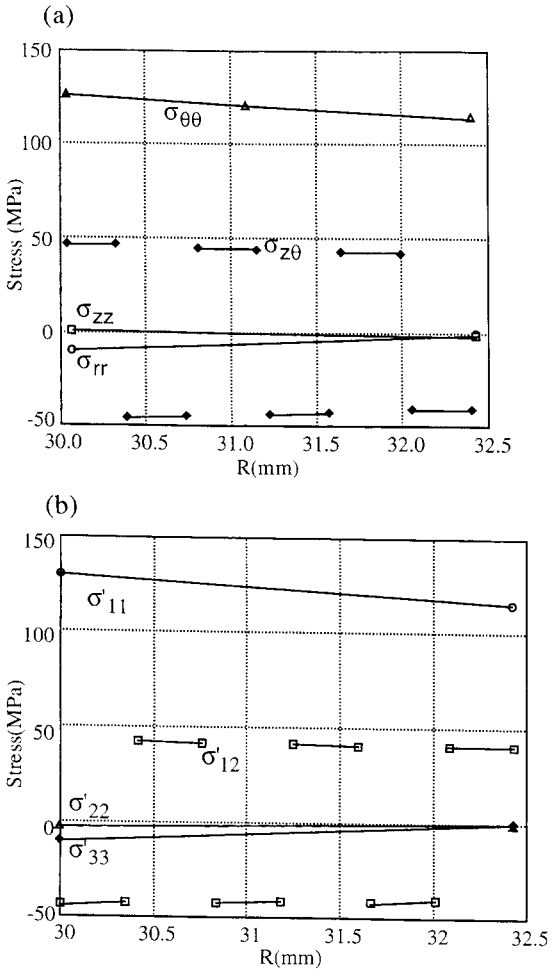


**Fig. 2.** (a) Stress distribution through the tube thickness expressed in global co-ordinates in a composite tube under pure internal pressure ($p = 10\,\text{MPa}$, $\sigma_{\theta\theta} = 120\,\text{MPa}$); (b) stress distribution through the tube thickness expressed in local co-ordinates in a composite tube under pure internal pressure ($p = 10\,\text{MPa}$, $\sigma_{\theta\theta} = 120\,\text{MPa}$).

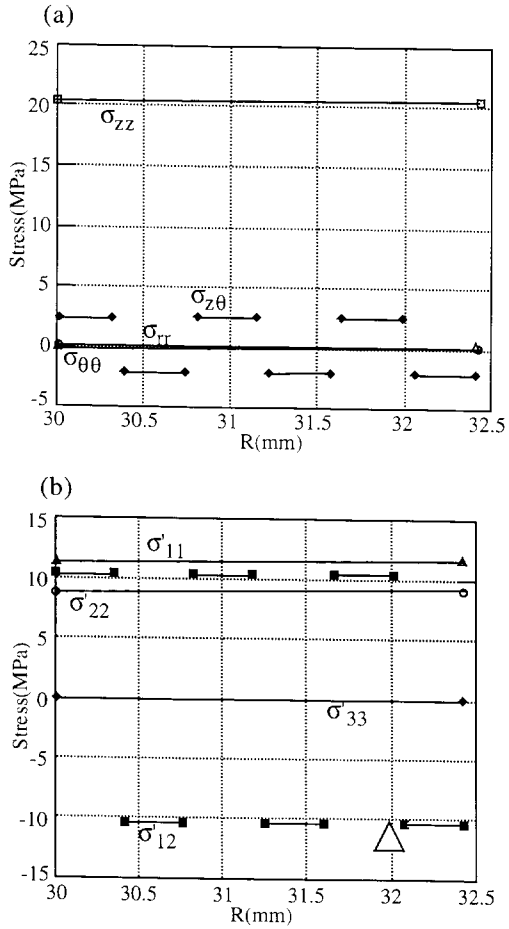


**Fig. 3.** (a) Stress distribution through the tube thickness expressed in global co-ordinates in a composite tube under pure tension ($F = 10\,\text{kN}$, $\sigma_{zz} = 20{\cdot}37\,\text{MPa}$); (b) stress distribution through the tube thickness expressed in local co-ordinates in a composite tube under pure tension ($F = 10\,\text{kN}$, $\sigma_{zz} = 20{\cdot}37\,\text{MPa}$).

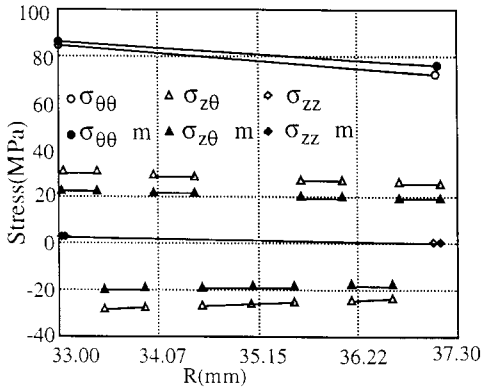


**Fig. 4.** Comparison with the adjusted laminated theory for composite tube $(55°/-55°/55°/-55°)_s$ (filled symbols: adjusted laminated theory).

are given in Tables 1 and 2. At least three values are needed to show the variation of the stresses in the thickness direction, at internal, middle thickness and external point. They exhibit some oscillation under pure internal pressure loading, being largest for $\sigma'_{11}$. The tensile $\sigma'_{22}$ may have direct effect on the critical load for transverse crack initiation, compared to compressive $\sigma'_{22}$ by other methods. The difference and the oscillation are not significant for tensile loading case.

*2.3.3 Comparison with finite-element results*

3D finite-element analysis was also conducted[20] in order to compare the results of the different methods. The whole tube was analysed to avoid possible boundary condition effects. The internal pressure and the tensile force imposed on the tube extremity are uniformly distributed on the corresponding faces. No other special boundary conditions were applied. It has been confirmed that the 3D numerical results can be used as reference of stress distribution for comparison purpose in varying the element size and the boundary conditions.[20] Tables 1 and 2 give the comparisons between the different methods. It is seen that the present analytical method agrees well with the 3D finite-element results.

### 2.4 Influence of a matrix layer

There is often an interply resin layer in filament-wound tubes.[1] In order to examine the effect of this layer on the stress distribution in the plies, we shall illustrate the influence on stress distribution (only in the case of pure internal pressure) of a 30 $\mu$m matrix layer located at the interface of the two internal plies by using the method described in Section 2.2. The results show that the presence of this matrix layer has little effect on the stress distribution in the tube (Fig. 5).

For a composite tube with a 30 $\mu$m matrix layer between the first and the second plies, under $p = 10$ MPa internal pressure, the stress components in the matrix layer are (in tube reference) $\sigma_{rr} = -8{\cdot}14$ MPa, $\sigma_{\theta\theta} = -16{\cdot}1$ MPa, $\sigma_{zz} = -12{\cdot}3$ MPa, $\sigma_{z\theta} = 0{\cdot}005$ MPa, while for the composite tube under pure tension ($F = 10$ kN, $\sigma_{ZZ} = 20{\cdot}37$ MPa), the stresses are $\sigma_{rr} = -0{\cdot}0023$ MPa, $\sigma_{\theta\theta} = -0{\cdot}65$ MPa, $\sigma_{zz} = 6{\cdot}4$ MPa, $\sigma_{z\theta} = 0{\cdot}005$ MPa. In the case of pure internal pressure, the absolute value of stress $\sigma_{zz}$ in the matrix layer is higher compared to the stresses in the composite layers.

## 3 COMPOSITE TUBE MACROSCOPIC BEHAVIOUR

### 3.1 Composite tube moduli

In this section, the composite tube will be treated as being made of a homogeneous material, and the constants of this effective homogeneous material will be determined from ply properties. This will enable us to establish a relationship between composite tube elastic constants and their ply properties. This also makes it possible to compare directly with experimental results.

Such research work has already been performed by many authors[21,22] with different simplifications. Usually in-plane elastic constants of a composite tube can be evaluated by classical laminate theory. Some simplifications are needed to derive the elastic constants throughout the tube thickness. In our analysis, the method proposed by Al-Khalil *et al.*[22] are used, which

**Table 1. Stress distribution from inner to external ply (internal pressure 10 MPa)**

| | $\sigma'_{11}$ | $\sigma'_{22}$ | $\sigma'_{33}$ | $\sigma'_{13}$ | $\sigma'_{23}$ | $\sigma'_{12}$ |
|---|---|---|---|---|---|---|
| Roy–Tsai model | 102—92 | −10——−10 | −10—0 | 0 | 0 | −40—40 |
| Classical laminate theory | 88·6—150—86·4 | 7——−3—7 | 0 | 0 | 0 | −45—40—45 |
| Present authors | 130·7—115·9 | −3·7——−2·2 | −10—0 | 0 | 0 | −42·1—39·9 |
| 3D finite-element | 130·3—119 | −3·5——−2·4 | −10—0 | 0 | 0 | −42·1—41·7 |

**Table 2. Stress distribution from inner to external ply (axial load 10 kN)**

| | $\sigma'_{11}$ | $\sigma'_{22}$ | $\sigma'_{33}$ | $\sigma'_{13}$ | $\sigma'_{23}$ | $\sigma'_{12}$ |
|---|---|---|---|---|---|---|
| Roy–Tsai model | 7 0—7·0 | 12—12 | 0 | 0 | 0 | 10——−10 |
| Classical laminate theory | 7·1—10—7 | 11·9—11·6—11·9 | 0 | 0 | 0 | 10·2——−10·2 |
| Present authors | 8·6—9·0 | 11·4—11·6 | 0 | 0 | 0 | 10·4——−10·3 |
| 3D finite-element | 8·6—9·0 | 11·5—11·6 | 0 | 0 | 0 | 11·3——−11·3 |

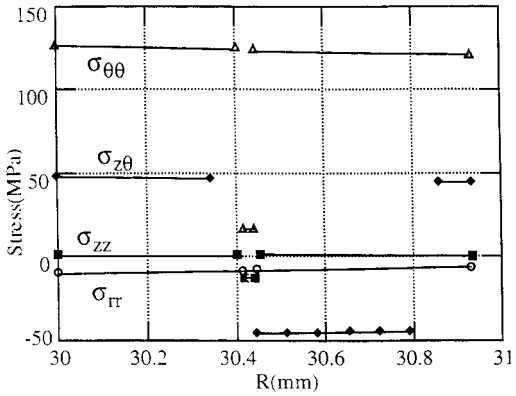


**Fig. 5.** Influence of a matrix layer on the stress distribution throughout the tube thickness expressed in the global tube reference ($p = 10$ MPa, $\sigma_{\theta\theta} = 120$ MPa).

includes: (1) normal stress throughout the tube thickness are constant, (2) out of plane shear strains are considered constant throughout the composite tube thickness. The reference system used here is: 11—radial direction, 22—hoop direction and 33—tube axis direction. The final results are reported in Appendix 2:

$$E_{22} = \frac{M}{C_{11}C_{33} - C_{13}C_{13}}, \quad E_{33} = \frac{M}{C_{11}C_{22} - C_{12}C_{12}},$$

$$E_{11} = \frac{M}{C_{22}C_{33} - C_{23}C_{23}}$$

$$\nu_{32} = -\frac{C_{12}C_{13} - C_{11}C_{23}}{C_{11}C_{22} - C_{12}C_{12}}, \quad \nu_{23} = -\frac{C_{12}C_{13} - C_{11}C_{23}}{C_{11}C_{33} - C_{13}C_{13}},$$

$$\nu_{12} = -\frac{\varepsilon_{22}}{\varepsilon_{11}} = -\frac{C_{12}C_{23} - C_{12}C_{33}}{C_{22}C_{33} - C_{23}C_{23}}$$

$$G_{23} = C_{44} - \frac{C_{14}C_{14}}{C_{11}}, \quad G_{13} = C_{55}, \quad G_{12} = C_{66} \tag{19}$$

where

$$M = C_{11}C_{22}C_{33} - C_{13}C_{13}C_{22} - C_{23}C_{23}C_{11} - C_{12}C_{12}C_{33} + 2C_{12}C_{13}C_{23},$$

$C_{ij}$ are the stiffness tensor of the ply in tube reference.

Application to the studied composite tube gives the results reported in Table 3, where the finite-element calculation,[20] micromechanical modelling[2] and experimental results[1] are also shown for comparison purposes. The ply stiffness is calculated by the Mori–Tanaka model.[12] A quick comparison shows an acceptable agreement for the results obtained by different methods, except for the value of $E_{33}$ which is the tube axis modulus. Experimental measurement gave a higher average value than the other methods with a large scatter.

### 3.2 Composite tube failure prediction

Prediction of the failure load for composite tubes is essential for their design and optimisation. In this section, a tentative using mesoscale criterion is presented to elucidate some obscurities between the model and reality.

*3.2.1 Mesoscopic criterion—maximum stress criterion*

A simple maximum stress criterion is used first to predict ply failure. If ply stresses in principle material reference exceed certain critical values, this individual ply fails. The corresponding load level is usually referred as first ply failure load. The criterion can be simply written as

$$-X_c \le \sigma'_{11} \le X_t, \quad -Y_c \le \sigma'_{22}, \quad \sigma'_{33} \le Y_t, \quad |\sigma'_{12}| \le S \tag{20}$$

The ply stresses $\sigma'_{11}, \sigma'_{22}, \sigma'_{33}$ and $\sigma'_{12}$ (in principle material axis) can be easily determined by either the finite-element method or the analytical method described previously. For the studied composite, the critical ply strengths were taken from similar materials studied by Hinton *et al.*[5] They are

$$X_c = 1280 \text{ MPa}, \quad X_t = 525 \text{ MPa}, \quad Y_t = 40 \text{ MPa}, \quad Y_c = 145 \text{ MPa}, \quad S = 73 \text{ MPa}$$

In this study, the stresses obtained by the analytical method are used as input to predict the composite tube failure load. The predicted results (first ply failure loads) together with the experimental ones are shown in Fig. 6.[1] It should be mentioned that the difference in the nature of those results, being the first-ply failure for the maximum stress criterion and microscale damage initiation for the experimental observations.

It is shown that, except for the case of pure tension, the predicted results underestimate the failure load compared to experimental values, especially for the combined loading case. This confirms the results by

**Table 3. Comparison of the elastic constants obtained by different methods**

| (GPa) | $E_{11}$ | $E_{22}$ | $E_{33}$ | $G_{12}$ | $G_{13}$ | $G_{23}$ | $\nu_{12}$ | $\nu_{23}$ | $\nu_{32}$ |
|---|---|---|---|---|---|---|---|---|---|
| 1 | | 19·0–25·0 | 9·8–10·9[a]<br>14·4–15·0[b] | | | | | 0·38–<br>0·40 | 0·59–<br>0·77 |
| 2 | 10·9 | 18·6 | 10·4 | 3·88 | 3·73 | 10·9 | 0·08 | 0·4 | 0·72 |
| 3 | | 19·225 | 10·1 | | | | | | |
| 4 | 11·36 | 20·9 | 10·48 | 3·89 | 3·73 | 13·1 | 0·04 | 0·419 | 0·839 |

1. Experimental results ([a]by 120 mm strain gauge, [b] by 50 mm extensometer),[1]; 2. Present authors; 3. 3D Finite-Element method,[20]; 4. Mori–Tanaka theory for orthotropic bi-plies.[2]

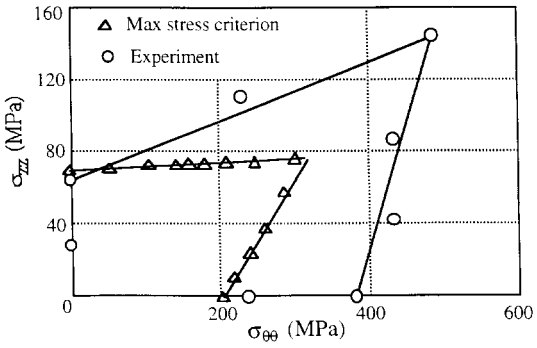


**Fig. 6.** Comparison between mesoscale prediction and experimental results.

Hinton *et al.*[5] that the five existing criteria (Tsai-Wu, Hill, etc.) give systematically underestimated prediction for first-ply failure load. This large discrepancy between the prediction and the tests could not be explained by the eventual scatter in the input data for criteria due to the composite tube manufacture and quality variation.

*3.2.2 Hashin's criterion*[23–25]

The basic idea of this criterion is that the failure of a laminate depends solely on the stresses in the failure plane. There are two modes of laminate failure: (1) fibre fracture mode, where the normal of the failure plane, is parallel to the fibre direction, and (2) matrix failure mode. Different criteria should be used for these two modes of failure. The predicted results are not improved compared to the maximum stress criterion.

## 4 DISCUSSION

### 4.1 Influence of microscale damage on stress distribution

The structural stress state analysis in this paper is generally based on an ideal distribution of fibres, without any microstructural damage. By micromechanical modelling, it is shown that microstructural damage was initiated for quite low stress levels. For example, $\sigma_{\theta\theta} = 120$ MPa for pure internal pressure loading with sliding at the interface by interfacial shear stress. This kind of sliding at the interface was observed on a prepolished free surface at about $\sigma_{\theta\theta} = -90$ MPa in compression and $\sigma_{\theta\theta} = 140$ MPa in hoop tensile tests.[26] The pure internal pressure stress state was produced with a recently developed notched ring test method while compression tests were made on cubes cut from the composite tubes.[27,28] In this section, the method presented in section 2 will be used to evaluate the stress redistribution for a tube with damage in the first ply or all six plies.

To simulate the tendency of the influence of the effect of this damage, one possibility is to use extremely low values of $E_{33}$ (transverse modulus) and $G_{23}$ (in-plane shear modulus) for the internal ply. They correspond, respectively, to the transverse cracking and in-plane sliding at the interface, along the fibres. According to the assumption of the micro-damage mechanisms involved, the ply could retain transverse isotropy or become an orthotropic material. Notable differences were found for tensile loading and internal pressure loading. For internal pressure loading ($p = 10$ MPa), the stresses were almost unaffected by the damage. The compressive transverse stress (perpendicular to the fibres) even increased its absolute value (from $-3$ MPa to $-11$ MPa), which prevented further propagation of eventual interfacial cracks. By contrast, for tensile loading ($F = 10$ kN), the stresses were comparatively more affected by the introduced damage. The transverse stress increased from 11 to 14 MPa, while the longitudinal stress along fibre increased from 8 to 11 MPa, and the transverse shear stress increased from 10 to 13 MPa.

To evaluate the effect of damage separately, only one mechanism is taken into consideration in the following simulation. Figure 7(a) shows the stresses, which are significantly affected, in the first ply for different $E_t$ values used in all six plies under tensile loading. The choice of first ply to display the stress evolution is only for clarity of expression. It is to simulate the case of matrix and transverse cracking in the whole thickness of tubes. It can be seen that $\sigma'_{11}$ and $\sigma'_{12}$ increase with decreasing transverse modulus, $E_t$, while $\sigma'_{22}$ decreases. Under pure internal pressure loading, the in-plane shear

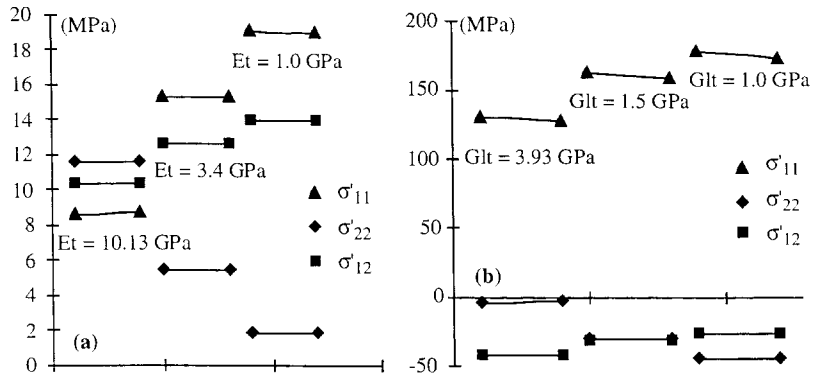


**Fig. 7.** Stress redistribution in the first ply under tensile and pure internal pressure loading as function of $E_t$ and $G_{lt}$ values in all six plies.

modulus is changed. The values of compressive $\sigma'_{22}$ increase from about $-4$ to $-44$ MPa.

The above results support the idea that under pure internal pressure loading, microscale damage is not detrimental to the loading-bearing capacity, but may affect the functional performance (leakage failure, for example). This also confirms the beneficial effect of using lined tubes in which the liner acts as a weepage barrier.[4,5] This also explains why in principal tensile loading regions, the tubes are more sensitive to microscale damage. The damage in this case develops more significantly under this kind loading. This idea will also be discussed in the Section 4.3.

### 4.2 Effect of local delamination

To evaluate the influence of local delamination on the macroscopical behaviour of tubes, as in the previous section, stress state analysis was performed by the finite-element method[20] on the same structure but introducing a very weak interply layer between the first two internal plies. The area of this weak layer was then increased progressively. The results showed that macroscopic behaviour was almost unaffected by this layer. To give an idea of that, $E_{\theta\theta}$ changed from 19225 MPa for the initial structure to 18443 MPa, with a generalised delamination (4% variation) and no change in $E_{zz}$.

A slightly larger change of elastic energy stored in the structure was found for propagation of delamination in the longitudinal direction than for propagation in the transverse direction. This is very small, however, indicating the insensitivity of the structure to damage due to delamination ($G_1 = 10\,\mathrm{J\ m^{-2}}$ compared to $G_{1c} = 100$–$150\,\mathrm{J\ m^{-2}}$). This conclusion agrees well with the absence of influence of introduced disks (see Section 3.2 of Part I of this series of papers)[1] on the macroscopical mechanical properties. They may, however, modify the local stress field and thus produce earlier local delamination (local debonding between the disk edge and matrix).

### 4.3 Improvement of the prediction of failure envelopes

To improve predicted results, the last-ply failure load concept can be utilised as the strength of composite tubes to calculate the corresponding load. The idea is as follows: for composite materials, the failure of one ply does not lead to catastrophic fracture of the composite material itself. The composite structure can still support an increasing load until a catastrophic failure occurs. To simulate stress redistribution due to a ply fracture, the failed ply's constants are degraded to represent the loss of its load-bearing capacity.

In our case, from micromechanical modelling it is shown that microstructural damage was initiated at quite low stress levels. For example, $\sigma_{\theta\theta} = 120$ MPa for pure internal pressure loading with sliding at the interface by interfacial shear stress. We shall now illustrate the crucial influence of some parameters on predicted results. We keep all other ply elastic constants unchanged and reduce $G_{lt}$ from 3·93 GPa to 1·5 GPa (more or less the matrix shear modulus). This change of ply shear modulus is chosen for two reasons: (1) ply shear stress and strain relationship is usually non-linear owing to the viscous nature of the matrix[29,30,4] and the longitudinal shear modulus predicted by elastic micromechanical model is usually higher; (2) In the internal-pressure-dominated region, the large shear stresses can somehow induce sliding along the fibre solidus matrix interface, which in turn will reduce this shear modulus.[2] The predicted results are shown in Fig. 8. It can be seen that the influence of this parameter on the predicted results is significant.

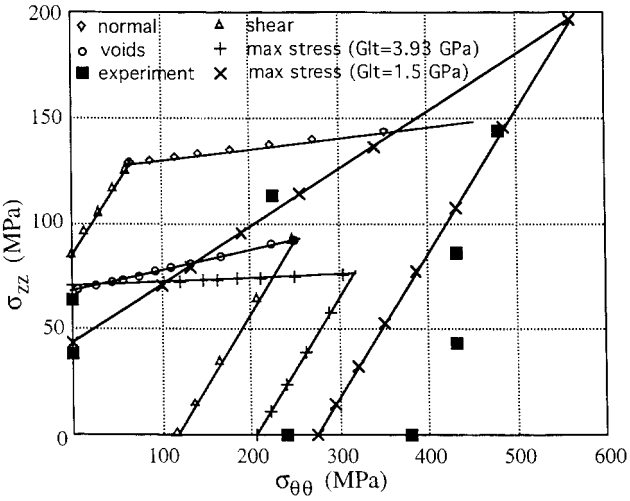


**Fig. 8.** Comparison between the different models (normal—interfacial failure by normal stress, shear—interfacial failure by shear stress, voids—cracking at voids, max stress—ply failure criteria) and the experimental results.[1]

## 5 CONCLUSION

The following conclusions can be drawn:

An analytical method for analysing the stress distribution in a laminated composite tube under combined load has been presented. Results predicted by this method agree with 3D finite-element analyses. This method is quite simple and can be combined with a micromechanics model to analyse the influence of fabrication defects (such as the presence of a matrix layer, fibre disorientation, voids, etc.) on stress distribution in the tube. Comparison was also made between the results obtained by different methods. It can be concluded that they all give similar stress distribution results under tensile loading, but different results under internal pressure loading.

A method for determining the elastic constants of a composite tube is also given. Comparison shows an acceptable agreement for the results obtained by different methods, except for the value of the tube axial modulus $E_{33}$. Experimental measurement gives a higher average value than the other methods with a large scatter.

Failure envelopes for our composite tube were predicted on the basis of different criteria at different scales (mesoscopic, microscopic). The predicted results in an internal-pressure-dominated region are conservative compared with experimental results. The possible improvement may reside in introducing a variation of the shear modulus to account for viscous matrix effects and interfacial sliding.

## ACKNOWLEDGEMENTS

The present research is supported by EDF-DER (Electricité de France). The authors are grateful to Drs F. Nagot, J. Le Bras and M. Lasne (EDF-MTC) for their discussions. The work was carried out in the laboratory MSS/MAT of Ecole Centrale Paris (CNRS URA 850). We would like to acknowledge the assistance rendered by our colleagues. Many thanks to the referee of our paper. Appropriate corrections and amendments are made based on his instructive comments and suggestions.

## REFERENCES

1. Bai, J. B., Seeleuthner, Ph. and Bompard, Ph., Mechanical behaviour of ±55° filament-wound glass-fibre/epoxy-resin tubes: Part I—Microstructure analyses and mechanical behaviour and damage mechanisms of composite tubes under pure tensile, pure internal pressure and combined loading. *Compos. Sci. Technol.*, 1997, **57**, 141–153.
2. Bai, J. B., Hu, G. K. and Bompard, Ph., Mechanical behaviour of ±55° filament-wound glass-fibre/epoxy-resin tubes: Part II—Micromechanical modelling of the damage initiation-competition of the different mechanisms. *Compos. Sci. Technol.*, 1997, **57**, 155–164.
3. Karayaka, M., Srinivasan, S., Miyase, A. and Wang, S. S., Leakage damage and failure of glass-fibre reinforced composite tubular vessels under combined internal pressure and axial loading. In *Proceedings of 10th Int. Conf. on Composite Materials (ICCM-10)* Vol. I. Whistler, B. C., Canada, 1995, pp. 747–754.
4. Carroll, M., Ellyin, F., Kujawski, D and Chiu, A. S., The rate-dependent behaviour of ±55° filament-wound glass-fibre/epoxy tubes under biaxial loading. *Compos. Sci. Technol.*, 1995, **55**, 391–403.
5. Hinton, M. J., Soden, P. D. and Kaddour, A. S., Strength of composite laminates under biaxial loads. In *Proceedings of 10th Int. Conf. on Composite Materials (ICCM-10)*, Vol. IV. Whistler, B.C., Canada, 1995, pp. 65–72.
6. Hull, D., Legg, M. J. and Spencer, B., Failure of glass/polyester filament wound pipe. *Composites*, 1978, **9**, 17–24.
7. Soden, P. D., Leadbetter, D., Griggs, P. R. and Eckold, G. C., The strength of a filament wound composite under biaxial loading. *Composites*, 1978, **9**, 247–250.
8. Foral, R. F. and Gilbreath, D. R., Delamination failure mode in filament wound composite tube. *ASTM STP 1012*, 1989, 313–325.
9. Soden, P. D., Kitching, R., Tse, P. C. and Tsavalas, Y., Influence of winding angle on the strength and deformation of filament-wound composite tubes subjected to uniaxial and biaxial loads. *Compos. Sci. Technol.*, 1993, **46**, 363–378.
10. Anderssen, R., Gradin, P. A., Gustafson, C.-G. and Nygard, P., Prediction of crack development and stiffness degradation in angle-ply filament wound pipes. *Proceedings of 10th Int. Conf. on Composite Materials (ICCM-10)*, 1995, **1**, I–407-14.
11. Frost, S. R., Predicting the long term fatigue behaviour of filament wound glass fibre/epoxy matrix pipes. *Proceedings of 10th Int. Conf. on Composite Materials (ICCM-10)*, 1995, **I**, I–649-56.
12. Joseph, E. and Pérreux, D., Fatigue behaviour of glass-fibre/epoxy-matrix filament-wound pipes: tension loading tests and results. *Compos. Sci. Technol.*, 1994, **52**, 469–480.
13. Levi, H., Ishai, O., Altus, E. and Sheinman, I., Mechanical performance of thin-walled tubular composite elements under uniaxial loading part 1: tensile behaviour. *Compos. Struct.*, 1995, **31**, 163–170.
14. Ishai, O., Levi, H., Altus, E. and Sheinman, I., Mechanical performance of thin-walled tubular composite elements under uniaxial loading part 2: compressive behaviour. *Compos. Struct.*, 1995, **31**, 171–175.
15. Jones, M. L. C. and Hull, D., Microscopy of failure mechanisms in filament-wound pipe. *J. Mater. Sci.*, 1979, **14**, 165–174.
16. Pagano, N. J., The stress field in a cylindrically anisotropic body under two-dimensional surface tractions. *ASME J. Appl. Mech.*, 1972, **39**, 791–796.
17. Roy, A. K. and Tsai, S. W., *Pressure vessels, Composite Design*. Think Composite Publisher, Dayton, OH, 1987, pp. 23-1–23-21.
18. Yuan, F. G., Composite laminated shells under internal pressure. *AIAA J.*, 1992, **30**, 1669–1672.
19. Sayir, M. B. and Motavalli, M., Fibre-reinforced laminated composite tubes with free ends under uniform internal pressure. *J. Mech. Phys. Solids*, 1995, 1691–1725.
20. Demianouchko, K. and Bai, J. B., Stress state analyses of a ±55° filament-wound composite tube with damage effect. *Compos. Struct.*, 1997, **37**, 233–240.
21. Sun, C. T. and Li, S., Three-dimensional effective elastic constants for thick laminates. *J. Compos. Mater.*, 1988, **22**, 629–639.
22. Al-Khalil, M. F. S. and Soden, P. D., Theoretical through-thickness elastic constants for filament-wound tubes. *Int. J. Mech. Sci.*, 1994, **36**, 49–62.
23. Hashin, Z., Failure criteria for unidirectional fiber composites. *ASME J. Appl. Mech.*, 1980, **47**, 329–334.
24. Puck, A., A failure criterion shows the direction, Kunststoffe combined with German. *Plastics*, 1992, **82**, 29–32.
25. Kroll, L. and Hufenbach, W., New proof of laminate design by a physically based failure criterion. In *Proceedings of 10th Int. Conf. on Composite Materials (ICCM-10)*, Vol. I. Whistler, B.C., Canada, 1995, pp. 715–722.
26. Dontchev, D., Bai, J. B., Djafari, V. and Bompard, Ph., Whitening phenomenon in a ±55° filament-wound glass-fibre/epoxy-resin tubes, submitted.
27. Arsène, A. and Bai, J. B., A new approach to measuring transverse properties of structural tubing by a ring test. *Int. J. of Testing and Evaluation*, 1996, 386–391.
28. Arsène, A. and Bai, J. B., A new approach to measuring transverse properties of structural tubing by a ring test—experimental investigation, *Int. J. Testing and Evaluation*, 1998, 26–30.
29. Maire, J. F., Etude théorique et expérimentale du comportement de matériaux composites en contraintes planes. Ph. D thesis, Université de Franche-Comté, 1992.

30. Le Moal, P., Pérreux, D. and Varchon, D., Viscoelastic behaviour of composite: comparison between a self-consistent model and experimental data. In *Proceedings of the 9th Int. Conf. on Composite Materials*, Vol. I. Madrid, Spain, 1993, pp. 715–722.

## APPENDIX 1

The relationship between the off-axis and axis compliance tensors

$$
\begin{aligned}
S_{11} &= S'_{33}\\
S_{12} &= S_{21} = S'_{13}\cos^2\theta + S'_{23}\sin\theta\\
S_{13} &= S_{31} = S'_{13}\sin^2\theta + S'_{23}\cos^2\theta\\
S_{14} &= S_{41} = 2\sin\theta\cos\theta(S'_{13} - S'_{23})\\
S_{22} &= S'_{11}\cos^4\theta + 2S'_{12}\cos^2\theta\sin^2\theta + S'_{22}\sin^4\theta\\
&\quad + S'_{66}\cos^2\theta\sin^2\theta\\
S_{23} &= S_{32} = \frac{1}{8}[S'_{11} + 6S'_{12} + S'_{22} - S'_{66}\\
&\quad - (S'_{11} - 2S'_{12} + S'_{22} - S'_{66})\cos 4\theta]\\
S_{24} &= S_{42} = \frac{1}{2}[S'_{11} - S'_{22} + (S'_{11} - 2S'_{12}\\
&\quad + S'_{22} - S_{66})\cos 2\theta]\sin 2\theta\\
S_{33} &= S'_{11}\sin^4\theta + 2S'_{12}\sin^2\theta\cos^2\theta + S'_{22}\cos^4\theta\\
&\quad + S'_{66}\sin^2\theta\cos^2\theta\\
S_{34} &= S_{43} = \frac{1}{2}[S'_{11} - S'_{22} - (S'_{11} - 2S'_{12}\\
&\quad + S'_{22} - S'_{66})\cos 2\theta]\sin 2\theta\\
S_{44} &= (S'_{11} - 2S'_{12} + S'_{22})\sin^2 2\theta + S'_{66}\cos^2 2\theta\\
S_{55} &= S'_{44}\cos^2\theta + S'_{55}\sin^2\theta\\
S_{56} &= S_{65} = (S'_{55} - S'_{44})\sin\theta\cos\theta\\
S_{66} &= S'_{55}\cos^2\theta + S'_{44}\sin^2\theta
\end{aligned}
\tag{A1}
$$

## APPENDIX 2

**Determination of composite tube elastic constants**

We have the following off-axis (tube reference) stress and strain relation in the form of a stiffness tensor for an individual ply:

$$
\begin{bmatrix}\sigma_{11}\\ \sigma_{22}\\ \sigma_{33}\\ \sigma_{23}\\ \sigma_{13}\\ \sigma_{12}\end{bmatrix} = \begin{bmatrix} C_{11} & C_{12} & C_{13} & C_{14} & & \\ C_{12} & C_{22} & C_{23} & C_{24} & & \\ C_{13} & C_{23} & C_{33} & C_{34} & & \\ C_{14} & C_{24} & C_{34} & C_{44} & & \\ & & & & C_{55} & C_{56}\\ & & & & C_{56} & C_{66}\end{bmatrix}\begin{bmatrix}\varepsilon_{11}\\ \varepsilon_{22}\\ \varepsilon_{33}\\ \varepsilon_{23}\\ \varepsilon_{13}\\ \varepsilon_{12}\end{bmatrix} \tag{A2.1}
$$

Now let us first consider in plane stresses $\sigma_{22}$, $\sigma_{33}$, $\sigma_{23}$, they can be related to the corresponding strains and $\sigma_{11}$ by:

$$
\begin{bmatrix}\sigma_{22}\\ \sigma_{33}\\ \sigma_{23}\end{bmatrix} = \begin{bmatrix} C_{22} - \frac{C_{12}C_{12}}{C_{11}} & C_{23} - \frac{C_{12}C_{13}}{C_{11}} & C_{24} - \frac{C_{12}C_{14}}{C_{11}}\\ C_{23} - \frac{C_{12}C_{13}}{C_{11}} & C_{33} - \frac{C_{13}C_{13}}{C_{11}} & C_{34} - \frac{C_{13}C_{14}}{C_{11}}\\ C_{24} - \frac{C_{12}C_{14}}{C_{11}} & C_{34} - \frac{C_{13}C_{14}}{C_{11}} & C_{44} - \frac{C_{14}C_{14}}{C_{11}}\end{bmatrix}\begin{bmatrix}\varepsilon_{22}\\ \varepsilon_{33}\\ \varepsilon_{23}\end{bmatrix} + \begin{bmatrix}\frac{C_{12}}{C_{11}}\\ \frac{C_{13}}{C_{11}}\\ \frac{C_{14}}{C_{11}}\end{bmatrix} \tag{A2.2}
$$

Laminate theory assumed that plane sections remain plane and perpendicular to the mid-plane of a laminate. For such a lamina, only under in-plane loads, the curvature and twist are negligible. So the lamina deformations are constant, that is

$$
\varepsilon_{22} = \varepsilon^0_{22}, \quad \varepsilon_{33} = \varepsilon^0_{33}, \quad \varepsilon_{23} = \varepsilon^0_{23} \tag{A2.3}
$$

where $\varepsilon^0_{22}$, $\varepsilon^0_{33}$, $\varepsilon^0_{23}$ indicate mid-plane strains.

Resultant in-plane forces are

$$
\begin{Bmatrix} N_2\\ N_3\\ N_{23}\end{Bmatrix} = \begin{bmatrix} A_{22} & A_{23} & A_{24}\\ A_{23} & A_{33} & A_{34}\\ A_{24} & A_{34} & A_{44}\end{bmatrix}\begin{Bmatrix}\varepsilon_{22}\\ \varepsilon_{33}\\ \varepsilon_{23}\end{Bmatrix} + \begin{Bmatrix} H_2\\ H_3\\ H_4\end{Bmatrix}\sigma_{11} \tag{A2.4}
$$

(here $\sigma_{11}$ is assumed constant throughout the tube thickness) where

$$
A_{ij} = \sum_{k=1}^{n}(w_{ij})_k t_k, \quad H_i = \sum_{k=1}^{n}\left(\frac{C_{1i}}{C_{11}}\right)_k t_k,
$$

$$
w_{ij} = C_{ij} - \frac{C_{1i}C_{1j}}{C_{11}}
$$

and $i, j = 2,3,4$, $t_k$ is the thickness of the $k^{\text{th}}$ ply.

For out of plane shear stresses, since $\varepsilon_{12}, \varepsilon_{13}$ are constant in tube thickness, the shear forces per unit width are given by

$$
\begin{aligned}
\begin{bmatrix} Q_5\\ Q_6\end{bmatrix} &= \sum_{k=1}^{n}\int_{x_1^{k-1}}^{x_1^k}\begin{bmatrix}\sigma_{13}\\ \sigma_{12}\end{bmatrix}\mathrm{d}x_1\\
&= \begin{bmatrix} A_{55} & A_{56}\\ A_{56} & A_{66}\end{bmatrix}\begin{bmatrix}\varepsilon^0_{13}\\ \varepsilon^0_{12}\end{bmatrix}
\end{aligned}
\tag{A2.5}
$$

and $A_{ij} = \sum_{k=1}^{n}(C_{ij})_k t_k$, for $i, j = 5, 6$.

For a symmetric angle ply tube ($\pm\theta$) with the same ply thickness, eqns (A2.4) and (A2.5) become

$$\begin{Bmatrix} N_2 \\ N_3 \\ N_{23} \end{Bmatrix} = \begin{bmatrix} A_{22} & A_{23} & 0 \\ A_{23} & A_{33} & 0 \\ 0 & 0 & A_{44} \end{bmatrix} \begin{Bmatrix} \varepsilon_{22} \\ \varepsilon_{33} \\ \varepsilon_{23} \end{Bmatrix} + \begin{Bmatrix} H_2 \\ H_3 \\ 0 \end{Bmatrix} \sigma_{11},$$

$$\begin{bmatrix} Q_5 \\ Q_6 \end{bmatrix} = \begin{bmatrix} A_{55} & 0 \\ 0 & A_{66} \end{bmatrix} \begin{bmatrix} \varepsilon_{13}^0 \\ \varepsilon_{12}^0 \end{bmatrix} \tag{A2.6}$$

with $A_{ij} = ntw_{ij}$ for $i,j = 2,3$ and for $i = j = 4$; $A_{ij} = ntC_{ij}$ for $i = j = 5,6$ $H_i = nt\frac{C_{1i}}{C_{11}}$ for $i = 2,3$.

Considering an axial load $\sigma_{11}$, and $N_2, N_3, N_{23}$ equal to zero, we have

$$w_{22}\varepsilon_{22} + w_{23}\varepsilon_{33} + \frac{C_{12}}{C_{11}}\sigma_{11} = 0 \tag{A2.7}$$

$$w_{23}\varepsilon_{22} + w_{33}\varepsilon_{33} + \frac{C_{13}}{C_{11}}\sigma_{11} = 0 \tag{A2.8}$$

From these two equations, we can express $\varepsilon_{22}, \varepsilon_{33}$ as a function of $\sigma_{11}$

$$\varepsilon_{22} = \frac{C_{13}C_{23} - C_{12}C_{33}}{M}\sigma_{11} \tag{A2.9}$$

$$\varepsilon_{33} = \frac{C_{12}C_{23} - C_{13}C_{22}}{M}\sigma_{11} \tag{A2.10}$$

where

$$M = C_{11}C_{22}C_{33} - C_{13}C_{13}C_{22} - C_{23}C_{23}C_{11} - C_{12}C_{12}C_{33} + C_{12}C_{13}C_{23}.$$

Replacing by $\varepsilon_{22}, \varepsilon_{33}$ by eqns (A2.9) and (A2.10), and with the help of the off-axis constitutive relation eqn (A2.1), we can derive the relation between $\sigma_{11}$ and $\varepsilon_{11}$ (here $\varepsilon_{23} = 0$, due to $N_{23} = 0$). This relation allows one to determine the out of plane modulus of the composite tube,

$$E_{11} = \frac{M}{C_{22}C_{33} - C_{23}C_{23}} \tag{A2.11}$$

Corresponding Poisson's ratios are

$$\nu = -\frac{\varepsilon_{22}}{\varepsilon_{11}} = -\frac{C_{12}C_{23} - C_{12}C_{33}}{C_{22}C_{33} - C_{23}C_{23}} \tag{A2.12}$$

Out of plane shear moduli $G_{13}$, $G_{12}$, can be simply estimated by applying a constant stress $\sigma_{13}$ or $\sigma_{12}$. We obtain finally

$$G_{13} = C_{55}, \quad G_{12} = C_{66} \tag{A2.13}$$

In plane moduli of the composite tube can be evaluated in the same way by applying respectively uniform tension or shear stresses on the $x_2$–$x_3$ plane. The final results are reported below

$$E_{22} = \frac{M}{C_{11}C_{33} - C_{13}C_{13}}, \quad E_{33} = \frac{M}{C_{11}C_{22} - C_{12}C_{12}},$$

$$E_{11} = \frac{M}{C_{22}C_{33} - C_{23}C_{23}}$$

$$\nu_{32} = -\frac{C_{12}C_{13} - C_{11}C_{23}}{C_{11}C_{22} - C_{12}C_{12}}, \quad \nu_{23} = -\frac{C_{12}C_{13} - C_{11}C_{23}}{C_{11}C_{33} - C_{13}C_{13}},$$

$$\nu_{12} = -\frac{\varepsilon_{22}}{\varepsilon_{11}} = -\frac{C_{12}C_{23} - C_{12}C_{33}}{C_{22}C_{33} - C_{23}C_{23}}$$

$$G_{23} = C_{44} - \frac{C_{14}C_{14}}{C_{11}}, \quad G_{13} = C_{55}, \quad G_{12} = C_{66} \tag{A2.14}$$